The Role of Internal and Effective Stresses in the Plastic Flow of Iron Single Crystals

W. A. SPITZIG AND A. S. KEH

The orientation and temperature dependence of the strain-rate sensitivity of the shear stress in iron single crystals were investigated at temperatures between 295° and 77°K. The results show that the shear stress-shear strain curves can be analyzed by separating the shear stress into internal and effective stress components. At all temperatures and for all orientations, work-hardening is associated with an increasing internal stress. The rapid increase in flow stress with decreasing temperature is a consequence of an increasing effective stress in agreement with implications derived from a thermally activated deformation mechanism. The only exception to this behavior was at 250°K where the work hardening is considerably different from that at 295°K. At 250°K the initial work-hardening rate is associated with both an increasing effective stress and an increasing internal stress.

IT is now generally accepted that the plastic deformation of metals is thermally activated and that the flow stress is composed of a relatively athermal component (τ_i), and a thermal component (τ^*). The athermal component is dependent on temperature only through the shear modulus, whereas the thermal component is both temperature and strain-rate dependent. Therefore, the shear stress (τ) at any point along the shear stress-shear strain curve can be expressed as:[1]

$$\tau = \tau^* + \tau_i \qquad [1]$$

The τ^* component of stress (referred to as an effective stress) is assumed to result from short-range obstacles to dislocation motion (*e.g.*, Peierls stress, impurity atoms and forest dislocations); thermal agitation assists in moving dislocations past these obstacles. The τ_i component of stress (referred to as an internal stress) is assumed to result from long-range obstacles to dislocation motion (*e.g.*, dislocation tangles and cell walls); thermal fluctuations are not significant in helping a dislocation overcome these obstacles.

If a single thermally activated mechanism controls the motion of dislocations, τ^* can be expressed as:[1-3]

$$\tau^* = \frac{1}{V^*}\left[\Delta H_0 + kT \ln\left(\frac{l^*\dot{\epsilon}}{\rho_m A b \nu^*}\right)\right] \qquad [2]$$

where

V^* = activation volume
ΔH_0 = activation enthalpy at $\tau^* = 0$
k = Boltzmann's constant
T = temperature
l^* = length of dislocation segment involved in the thermal activation
$\dot{\epsilon}$ = strain rate
ρ_m = mobile dislocation density
A = area in glide plane swept out by a dislocation per successful fluctuation
b = Burgers vector of dislocation
ν^* = frequency of vibration of the dislocation segment of length l^*.

W. A. SPITZIG is Senior Scientist, Edgar C. Bain Laboratory, U. S. Steel Corp., Monroeville, Pa. A. S. KEH, formerly with Edgar C. Bain Laboratory, is deceased.

Manuscript submitted May 14, 1970.

Eq. [2] assumes that the entropy of activation is negligibly small, in agreement with previous results obtained from the iron single crystals used in this investigation.[4] At a constant strain rate ($\dot{\epsilon}$) the factors l^*, A, and ν^* are taken as constant at a given temperature, and the mobile dislocation density (ρ_m) is believed to determine τ^*.[1,2,5] Therefore, τ^* is expected to increase, decrease or remain constant with strain as ρ_m decreases, increases or remains constant, respectively, provided that the parameter m^*, given by:[6-8]

$$m^* = \frac{V^*\tau^*}{kT} \qquad [3]$$

remains constant with strain.

The internal stress (τ_i) is usually related to the total dislocation density (ρ) as:[2,3,9]

$$\tau_i = \alpha \mu b \rho^{1/2} \qquad [4]$$

where

α = constant
μ = shear modulus.

Since τ_i is relatively independent of temperature, the strong temperature dependence of the flow stress in bcc metals is primarily a consequence of an increasing τ^* with decreasing temperature.[1,2,10,11] Work-hardening results from long-range obstacles and is associated with an increasing τ_i with increasing strain.[1,2,10,11]

The purposes of this investigation were to analyze the orientation and temperature dependence of plastic flow in iron single crystals in terms of internal and effective stresses, and to compare the results with the implications of a thermally activated deformation mechanism. Such an extensive analysis of plastic flow in terms of internal and effective stresses has been lacking. The orientation and temperature dependence of plastic flow and activation parameters in these iron crystals have been discussed previously.[4,12]

MATERIAL AND PROCEDURES

The material used in this investigation was "Plastiron" Type 104A, supplied by the Glidden Co. The composition of the iron after vacuum melting and

Table I. Composition of Base Iron, in Wt Pct

C	Mn	P	S	Si
0.002	0.01	0.002	0.002	0.004
Cu	Ni	Cr	Mo	V
0.005	0.008	0.002	0.005	0.005
Ti	Al	Co	N	O
0.005	0.002	0.004	0.001	0.004

vacuum carbon deoxidation is shown in Table I. A single crystal with dimensions 2.5 by 0.25 by 23 cm was grown by the strain anneal technique, then treated at 1125°K in a ZrH_2 system[13] for 360 hr. This treatment reduced the carbon and nitrogen contents to below 10 ppm and the oxygen content to 10 ppm. Single-crystal tensile specimens with a gage length of 1.5 cm and a rectangular cross section of approximately 0.25 by 0.20 cm were prepared by spark cutting, followed by chemical and electrolytic polishing. The six orientations investigated are shown in Fig. 1. The Schmid factor is about 0.5 for all these orientations.

Tension tests were performed on an Instron machine at a base crosshead speed of 0.025 cm per min, which corresponds to a nominal strain rate of 5.6×10^{-4} sec^{-1}. Strain-rate change tests were conducted at crosshead speeds of 0.025 and 0.125 cm per min (nominal strain rate 2.8×10^{-3} sec^{-1}). At 295° and 250°K, strain-rate change tests were also conducted at crosshead speeds of 0.005 (nominal strain rate 1.12×10^{-4} sec^{-1}) and 0.025 cm per min. All changes in stress as a result of the strain-rate changes were measured for upward changes in strain rate. A push-button gear box was used for the strain-rate changes, and load suppression techniques were used to expand the load scale during strain-rate changes.

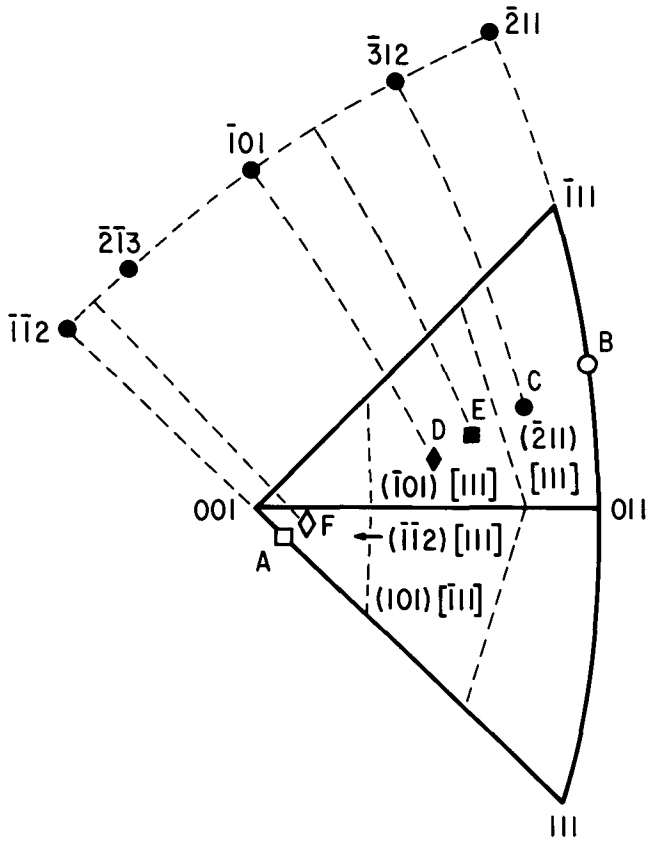

Fig. 1—Orientation of specimens.

Controlled temperature liquid baths were used at 250°, 195°, and 143°K. The temperature 143°K was selected so that twinning would not occur during deformation. Crystals tested at 77°K were prestrained 5 pct at 295°K to suppress twinning during subsequent deformation. Shear stresses and shear strains were calculated from the appropriate single[14] and double slip[14,15] formulae, using the slip planes that operate at the several temperatures in these crystals.[16]

The applied shear stress (τ) was divided into τ^* and τ_i components, Eq. [1], derived from strain-rate cycling experiments. During a strain-rate change the ratio of the change in strain rate to the change in shear stress is usually defined by the parameter m:

$$m = \left(\frac{\partial \ln \dot{\epsilon}}{\partial \ln \tau}\right)_T \qquad [5]$$

It has been suggested that the exponent m^* in the empirical relation between dislocation velocity (v) and shear stress ($v = A\tau^{m^*}$)[6,17] can be determined from strain-rate cycling tests by the relation:[2,6,8]

$$m^* = \left(\frac{\partial \ln \dot{\epsilon}}{\partial \ln \tau^*}\right)_T \qquad [6]$$

where m and m^* are related by:

$$m^* = m - \tau_i \left(\frac{\partial \ln \dot{\epsilon}}{\partial \tau}\right)_T \qquad [7]$$

Eq. [6] is obtained from the dislocation velocity-stress relation[6] and the strain rate-velocity relation ($\dot{\epsilon} = \alpha \rho_m b v$) by assuming that the density (ρ_m) of mobile dislocations and the internal stress remain constant during a strain-rate cycle. Eq. [3] is just a restatement of Eq. [6]. Eq. [7] shows that $m^* = m$ when the internal stress (τ_i) is zero. The agreement between the values obtained for m^* from strain-rate change tests and those from other techniques (*e.g.*, etch pit studies or internal friction) has been discussed in considerable detail and will not be considered here.[18]

If double strain-rate cycling techniques are used, Eq. [6] can be expressed as:[6]

$$m^* = \frac{\ln(\dot{\epsilon}_2/\dot{\epsilon}_1)}{\ln[(\tau_2 - \tau_i)/(\tau_1 - \tau_i)]} = \frac{\ln(\dot{\epsilon}_3/\dot{\epsilon}_2)}{\ln[(\tau_3 - \tau_i)/(\tau_2 - \tau_i)]} \qquad [8]$$

where τ_1, τ_2, and τ_3 are the shear stresses at strain rates $\dot{\epsilon}_1$, $\dot{\epsilon}_2$, and $\dot{\epsilon}_3$, respectively. If the strain-rate ratios $\dot{\epsilon}_2/\dot{\epsilon}_1$ and $\dot{\epsilon}_3/\dot{\epsilon}_2$ are made equal and m^* is assumed to be constant during the strain-rate cycles, τ_i is given by:

$$\tau_i = \frac{\tau_1 \tau_3 - \tau_2^2}{\tau_1 + \tau_3 - 2\tau_2} \qquad [9]$$

Therefore, the internal stress can be evaluated from double strain-rate cycling tests, the effective stress

can be calculated from Eq. [1] and m^* can be obtained from either part of Eq. [8]. The magnitude of m^* was the same regardless of which part of Eq. [8] was used. This technique was used at 295° and 250°K for the nominal strain rates $\dot{\epsilon}_1 = 1.12 \times 10^{-4}$, $\dot{\epsilon} = 5.6 \times 10^{-4}$, and $\dot{\epsilon}_3 = 2.8 \times 10^{-3}$ sec^{-1}.

The double strain-rate cycling technique appears to be limited to values of m^* of about 10 or less. At greater values, the differences in stress increments in the two strain-rate cycles become of the order of the experimental uncertainty.[7] Therefore, the procedure used at 195°, 143°, and 77°K to evaluate τ^* and τ_i as a function of strain was to calculate m^* from Eq. [3] using τ^* and V^* values obtained at the critical resolved shear stress (CRSS). The value of τ^* at the CRSS was obtained in the following manner. The internal stress at zero strain (τ_i^0) at 295° and 250°K was obtained by extrapolating the τ_i and τ^* data from the double strain-rate cycling technique to zero strain. The magnitude of τ_i^0 was about 50 kgf/cm^2 and appeared to be independent of orientation and temperature. A value of 50 kgf/cm^2 was also obtained for τ_i^0 for iron single crystals similar to orientations D and B, when the CRSS at the temperature where the strain-rate sensitivity became zero (*i.e.*, $\tau^* = 0$) was used for τ_i^0.[19] Therefore, 50 kgf/cm^2 was used for τ_i^0 to obtain the magnitude of τ^* at the CRSS (taken as the proportional limit) at 195° and 143°K. At 77°K the value of τ_i at 5 pct strain at 295°K was taken for τ_i^0. The values of the activation volume were reported previously[4] and were obtained from the relation:

$$V^* = kT\left(\frac{\partial \ln \dot{\epsilon}}{\partial \tau}\right)_T \qquad [10]$$

Using the values of τ^* and V^* at the CRSS in Eq. [3] gives the calculated values for m^* shown in Table II. Substituting Eq. [10] for V^* in Eq. [3]:

$$\frac{m^*}{\tau^*} = \left(\frac{\partial \ln \dot{\epsilon}}{\partial \tau}\right)_T \qquad [11]$$

and using Eq. [11] in Eq. [7] results in:

$$\tau^* = \frac{m^*}{m}\tau \qquad [12]$$

The variation of m as a function of orientation, temperature, and strain in these iron crystals has been reported previously.[4] Therefore, τ^* can be calculated as a function of strain from Eq. [12] using the experimental data for m and τ as a function of strain and the assumption that m^* is independent of strain, and τ_i can be obtained from Eq. [1].

RESULTS

The maximum resolved shear stress planes (MRSSP) of the six orientations investigated and the theoretical boundaries where the various {110} and {112} slip planes are expected to operate are shown in Fig. 1. Orientations A and F are referred to a different reference triangle so that all of the orientations have the [111] primary slip direction. Slip line studies show that orientations A, D, and B slip on the $(\bar{1}\bar{1}2)$, $(\bar{1}01)$, and $(\bar{2}11)$ planes, respectively, at all five temperatures.[16] Orientation E slips on the $(\bar{1}01)$ plane at ambient and lower temperatures, and orientation F slips on the $(\bar{1}\bar{1}2)$ plane at 195°K and below. Orientation C appears to slip on the $(\bar{3}12)$ plane at 195°K and below. At 295° and 250°K the slip planes for orientations F and C deviate from the MRSSP toward the $(\bar{1}01)$ plane.

Fig. 2 shows the shear stress-shear strain curves for orientations A, D, and B at 295°K, where three-

Table II. Calculated Values of m^*

Temperature, °K	Orientation					
	A	*F*	*D*	*E*	*C*	*B*
195	14	12	11.5	10	10	9
143	30	27	24	24	22	20.5
77	63		51			49

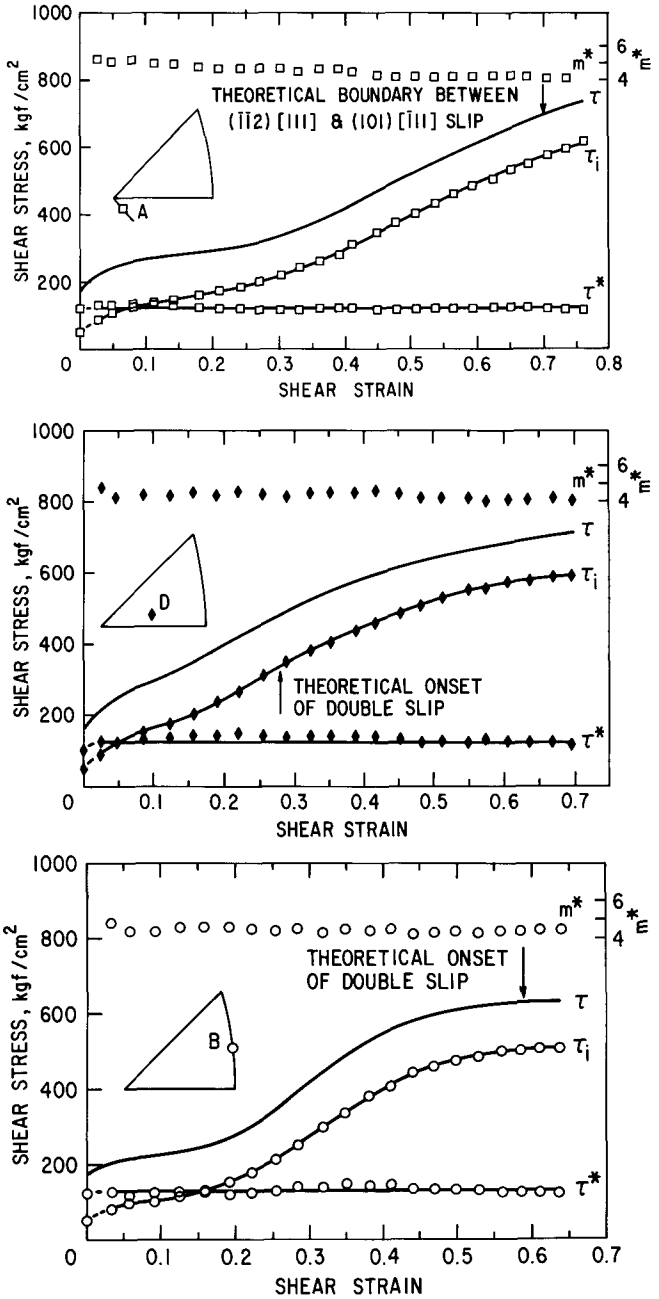

Fig. 2—Variation of applied stress (τ), internal stress (τ_i), effective stress (τ^*), and $m^* = \partial \ln \dot{\epsilon} / \partial \ln \tau^*$ with strain for orientations A, D, and B at 295°K ($\dot{\epsilon} = 5.6 \times 10^{-4}$ sec^{-1}).

stage hardening is prominent, divided into τ_i and τ^* components of stress. The m^* values are also shown as a function of strain. The curves for orientations F, E, and C are similar to those for orientations A, D and B, respectively. The shear strain where double slip should begin is shown by an arrow on the curves for orientations D and B. For orientation A the strain where slip should begin on the $(101)[\bar{1}11]$ slip system is shown on the curve. However, this is not a double slip position in the usual sense because the tensile axis continues to migrate away from the [001] pole.[15,16]

The curves in Fig. 2 show that both τ^* and m^* are independent of strain and orientation at 295°K. The increase in shear stress with shear strain (*i.e.*, work-hardening) is associated with an increase in the τ_i component of stress. In the third stage of the shear stress-shear strain curve τ_i is about 0.8 τ. The values of τ_i and τ^* at the shear stress axis in Fig. 2, and in all the other figures, are a result of extrapolating the τ^* and τ_i data to zero strain as discussed in the foregoing.

Fig. 3 shows the variation of τ_i, τ^*, and m^* with shear strain at 250°K for the six orientations investigated. Double strain-rate cycling techniques were used to evaluate τ_i and m^*. Comparison of the shear stress-shear strain behavior at 250°K with that at

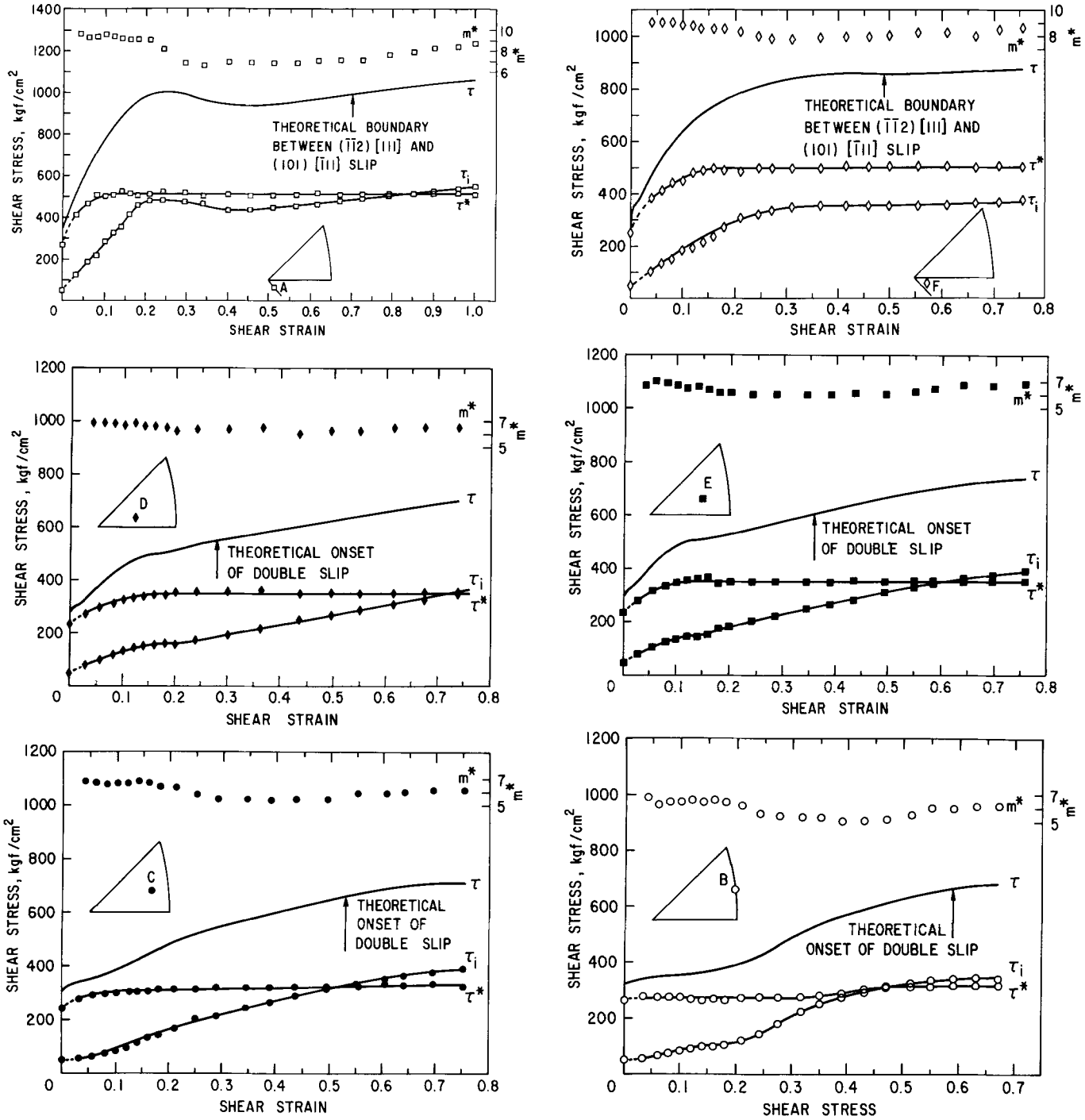

Fig. 3—Variation of applied stress (τ), internal stress (τ_i), effective stress (τ^*), and $m^* = \partial \ln \dot{\epsilon} / \partial \ln \tau^*$ with strain for orientations A, F, D, E, C, and B at 250°K ($\dot{\epsilon} = 5.6 \times 10^{-4} \text{sec}^{-1}$).

295°K shows that there is a drastic difference in the work-hardening behavior of orientations A and F (compare Figs. 2 and 3). The effective stress at 250°K increases up to strains of about 0.1 before becoming independent of strain. Orientation B is the only exception, but τ^* appears to increase during the third stage of three-stage hardening for this orientation. The constant value of τ^* decreases continously from 510 to 270 kgf/cm^2 on going from orientation A to B. However, at the larger strains τ is also about twice as large for orientation A as for orientation B.

At 250°K the initial work-hardening rate is associated with both an increasing τ^* and τ_i for orientations A, F, D, E, and C, with τ^* increasing most for orientations A and F, Fig. 3. At shear strains greater than about 0.1, a changing τ_i is associated with any hardening or softening. The increase in τ at 250°K over that at 295°K results from an increase in τ^*. At the larger strains τ^* and τ_i are about equal for all the orientations.

The m^* values at 250°K are orientation dependent and decrease continuously from 9.5 for orientation A to 6.5 for orientation B, Fig. 3. In addition, m^* appears to be constant only up to a shear strain of about 0.2. At larger shear strains m^* decreases and then increases again to about its initial value. This behavior is most pronounced for orientation A where m^* decreases from about 9.5 to 7 when work-softening occurs, Fig. 3.

Fig. 4 shows the shear stress-shear strain curves of orientations A, D, and B at 195° and 143°K. Fig. 5 shows the shear stress-shear strain curves of orientations A, D, and B at 77°K. Orientations F, E, and C are similar in behavior to orientations A, D, and B, respectively. The τ^* values in these figures were calculated from Eq. [12], using the values of m^* shown in Table II, as discussed in the foregoing. The value of m^* decreases on going from orientation A to B at 195°, 143°, and 77°K in accord with the results at 250°K. At 195°K and below, the calculated values of τ^* are independent of strain for all of the orientations. This accords with the assmption that m^* is independent of strain in evaluating τ^* from Eq. [12].

At 195°K τ^* ranges from about 750 kgf/cm^2 (orientation A) to about 650 kgf/cm^2 (orientations B and D, Fig. 4). At 143° and 77°K, τ^* is largest for orientation B (1400 and 2550 kgf/cm^2, Figs. 4 and 5) and smallest for orientation D (1100 and 1900 kgf/cm^2, Figs. 4 and 5). For all orientations work-hardening is associated with an increasing τ_i. The large increase in τ at these lower temperatures results from an increasing τ^*.

If τ^* is calculated as a function of strain at 295° and 250°K using Eqs. [3] and [12], as was done at 195°, 143°, and 77°K, the results are similar to those obtained using the double strain-rate cycling procedure. That is, τ^* remains constant with strain and τ_i is associated with any hardening or softening. The only difference is that the values calculated for m^* from Eq. [3] at 295° and 250°K (m^* = 3 to 4 and 5 to 6, respectively), are smaller than those obtained from double strain-rate cycling. As a result τ^* is slightly smaller and τ_i is slightly larger than shown in Figs. 2 and 3. However, both techniques predict the same characteristic behavior for τ^* and τ_i.

The differences between the two techniques results from the difficulty in evaluating V^* at the CRSS at 295°

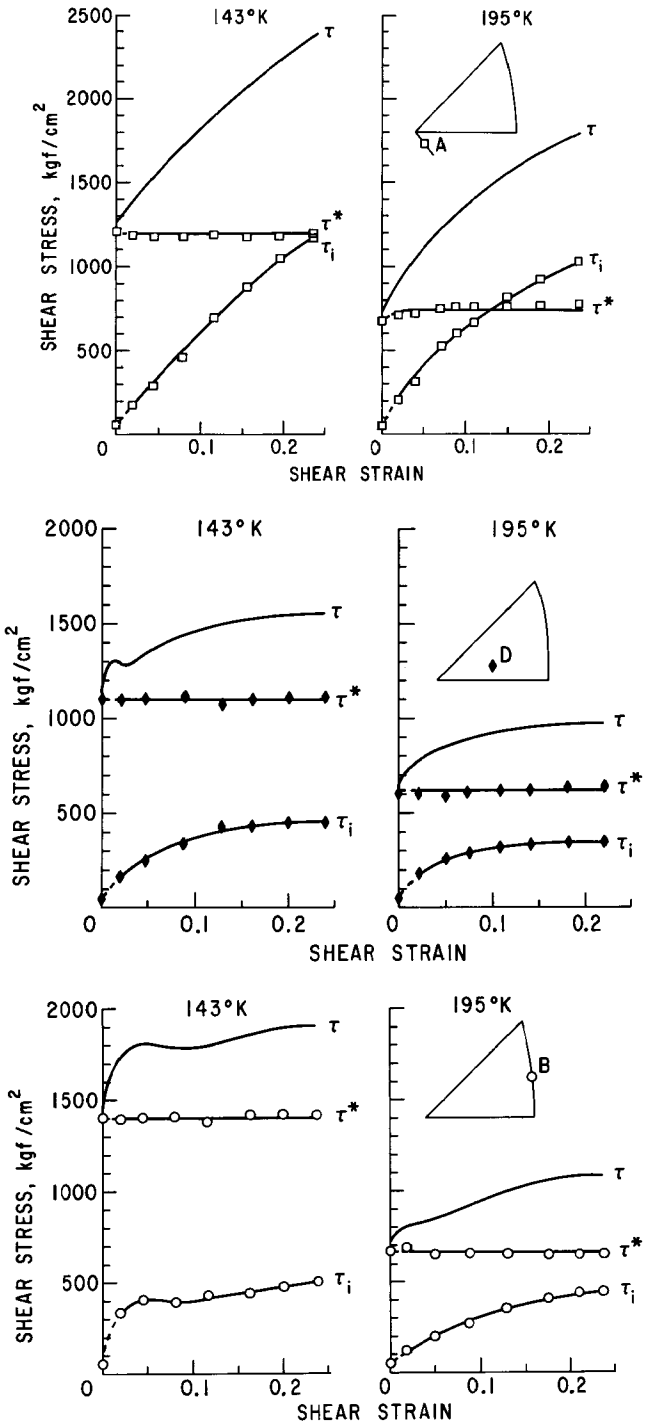

Fig. 4—Variation of applied stress (τ), internal stress (τ_i), and effective stress (τ^*) with strain for orientations A, D, and B at 195° and 143°K ($\dot{\epsilon}$ = 5.6 × 10^{-4} sec^{-1}).

and 250°K where V^* decreases with strain,[4] and also because values of V^* calculated from Eq. [10] are only reliable at low temperatures where τ^* is large.[20] Therefore, the values of m^* calculated from Eq. [3] are expected to be accurate only at low temperatures.

DISCUSSION OF RESULTS

The results of this study show that analysis of the shear stress-shear strain curves of iron single crystals in terms of effective stresses (τ^*) and internal stresses (τ_i) is consistent with the implications of a

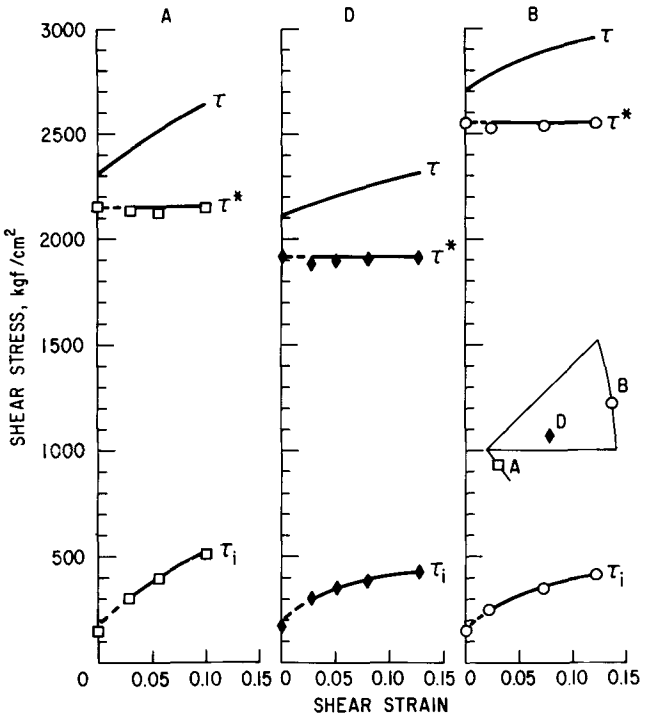

Fig. 5—Variation of applied stress (τ), internal stress (τ_i), and effective stress (τ^*) with strain for orientations *A*, *D*, and *B* at 77°K after 5 pct prestrain at 295°K ($\dot{\epsilon} = 5.6 \times 10^{-4}$ sec^{-1}).

thermally activated flow mechanism. At all temperatures and for all orientations, work-hardening is associated with an increasing internal stress. The rapid increase in flow stress with decreasing temperature is a consequence of an increasing effective stress. These results are in accord with previous less extensive investigations of iron.[2,10,11] In addition, both the effective stress and the parameter m^* are independent of strain. However, they are orientation dependent at 250°K and below. The orientation and temperature dependence of τ^* and m^* have been discussed previously.[4]

The only apparent deviations from the predicted behavior are at 250°K where the work-hardening behavior changes considerably from that at 295°K, and the effective stress also increases during the initial work-hardening (shear strains up to about 0.1) for orientations *A*, *F*, *D*, *E*, and *C*. In addition, m^* seems to be independent of strain only up to a shear strain of about 0.2 at 250°K.

This apparent deviation from a strain-independent m^* seems to coincide with a region in the shear stress-shear strain curve where the work-hardening rate is changing, and is most prominent for orientation *A* where work-softening is occurring, Fig. 3. Because work-hardening is associated with an increasing internal stress, the assumption of a constant τ_i during the strain-rate cycles in calculating m^*, Eq. [8], in a region of the shear stress-shear strain curve where the work-hardening rate is changing, may be unreasonable. That is, the apparent decrease in m^* may be a consequence of τ_i not remaining constant during the strain-rate cycles. In addition, the variation in m^* from a mean value is only ±1.5 for orientation *A* and less than ±1 for the other orientations which is about the expected experimental variation in m^*. Therefore, no significance should be attached to the apparent decrease in m^* at 250°K because the reality of the effect is questionable.

The tendency for τ^* to increase during the initial stages of straining at 250°K for orientations *A*, *F*, *D*, *E*, and *C* can be related to a decreasing density (ρ_m) of mobile dislocations, Eq. [2]. This decreasing density contributes to the work-hardening rate at the lower strains. At shear strains greater than about 0.1, τ^* becomes constant, but its value is significantly greater than the value of τ^* at the CRSS. This effect is most pronounced for orientations *A* and *F*, which have the largest work-hardening rates, Fig. 3. For orientation *B*, τ^* appears to increase during the third stage of three-stage hardening, indicating that the mobile dislocation density is decreasing at the larger strains. However, this behavior is not observed at 295°K where three-stage hardening is most prominent, Figs. 2 and 3.

The large work-hardening rates for orientations *A* and *F* at low strains at 250°K are associated about equally with an increasing τ^* and τ_i. The larger work-hardening rates for orientations *A* and *F*, as compared to orientations *B* and *C*, agree with recent dislocation density determinations in iron single crystals which show that the dislocation density for an [001] orientation is about ten times greater than that for an [011] orientation at 295°K.[21] At 195°K the dislocation density for an [001] orientation is about one hundred times greater than that for an [011] orientation.[21] The present results indicate that a decreasing density of mobile dislocations is also an important factor in the large work-hardening rates for orientations near [001]. However, a decreasing ρ_m seems to contribute to the initial work-hardening rate only at 250°K where orientations near [001] undergo a drastic change in deformation behavior (compare Figs. 2 and 3).

According to Eq. [2] a constant τ^* during deformation indicates that ρ_m remains constant with strain, provided m^*, Eq. [3], remains constant. Therefore, except for the deviations at small strains at 250°K, the mobile dislocation density in these iron crystals is expected to remain constant during deformation. If Eq. [2] is used to estimate the changes in ρ_m as a result of τ^* increasing at 250°K, by assuming that all the quantities except ρ_m are constant, ρ_m should decrease by two orders of magnitude for orientation *A* in the low-strain region, Fig. 3, and by a factor of 5 for orientation *B* in the high-strain region, Fig. 3. Although differences are expected in ρ_m for orientations near [001] and [011], because of differences in dislocation densities,[21] it is not possible to prove or disprove the reasonableness of the predicted changes.

Analyzing the shear stress-shear strain curves in terms of internal and effective stress components is phenomenological and only shows that the orientation and temperature dependence of deformation of iron single crystals agrees with the implications of a thermally activated deformation mechanism. However, from this type of analysis alone it is not possible to decide which of the proposed thermally activated mechanisms controls low-temperature deformation of iron. All of the theories predict that the increase in flow stress with decreasing temperature arises from the larger effective stress needed to move dislocations at low temperatures where there is a decrease in the thermal energy available for dislocation

movement.[22] However, previous work[4] on these iron crystals shows that the orientation and temperature dependence of the CRSS and the strain-rate sensitivity of the flow stress are in good agreement with the thermally activated flow theory of Dorn and Rajnak.[23]

CONCLUSIONS

1) The orientation and temperature dependence of the shear stress-shear strain curves of iron single crystals can be analyzed in terms of internal and effective stress components.

2) Work-hardening in iron single crystals is associated with an increasing internal stress.

3) The rapid increase in flow stress with decreasing temperature is a consequence of an increasing effective stress, consistent with implications derived from a thermally activated deformation mechanism.

ACKNOWLEDGMENTS

The benefit of many informative discussions with J. C. M. Li is gratefully acknowledged.

REFERENCES

1. H. Conrad: *Iron and Its Dilute Solid Solutions*, C. W. Spencer and F. E. Werner eds., pp. 315-39, Interscience, New York, 1961.
2. J. T. Michalak: *Acta Met.*, 1965, vol. 13, pp. 213-22.
3. D. J. Bailey and W. F. Flanagan: *Phil. Mag.*, 1967, vol. 15, pp. 43-49.
4. W. A. Spitzig and A. S. Keh: *Acta Met.*, 1970, vol. 18, pp. 1021-33.
5. D. J. Bailey and W. F. Flanagan: *Phil. Mag.*, 1969, vol. 19, pp. 1093-1103.
6. J. C. M. Li: *Can. J. Phys.*, 1967, vol. 45, pp. 493-509.
7. J. W. Christian: *Acta Met.*, 1967, vol. 15, pp. 1257-58.
8. K. R. Evans, D. J. Bailey, and W. F. Flanagan: *Phys. Stat. Sol.*, 1967, vol. 22, pp. 607-16.
9. J. C. M. Li: *Direct Observation of Imperfections in Crystals*, J. B. Newkirk and J. H. Wernick eds., pp. 234-38, Interscience, New York, 1962.
10. M. Nagumo and H. Matsuda: *Trans. Jap. Inst. Metals*, 1968, vol. 9 (Suppl.), pp. 885-89.
11. H. Yada and H. Mimura: *J. Phys. Soc. Jap.*, 1968, vol. 24, pp. 1269-78.
12. W. A. Spitzig and A. S. Keh: *Acta Met.*, 1970, vol. 18, pp. 611-22.
13. D. F. Stein, J. R. Low, Jr., and A. U. Seybolt: *Acta Met.*, 1963, vol. 11, pp. 1253-62.
14. E. Schmid and W. Boas: *Plasticity of Crystals*, pp. 55-68, Chapman and Hall, London, 1968.
15. D. K. Bowen and J. W. Christian: *Phil. Mag.*, 1965, vol. 12, pp. 369-78.
16. W. A. Spitzig and A. S. Keh: *Met. Trans.*, 1970, vol. 1, pp. 2751-57.
17. W. G. Johnston and J. J. Gilman: *J. Appl. Phys.*, 1959, vol. 30, pp. 129-44.
18. F. R. N. Nabarro and H. Conrad: *Dislocation Dynamics*, A. R. Rosenfield *et. al.* eds., pp. 475-84, McGraw-Hill, New York, 1968.
19. A. S. Keh and Y. Nakada: *Can. J. Phys.*, 1967, vol. 45, pp. 1101-20.
20. J. C. M. Li: *Dislocation Dynamics*, A. R. Rosenfield *et. al.* eds., pp. 87-116, McGraw-Hill, New York, 1968.
21. S. Ikeda: *J. Phys. Soc. Jap.*, 1969, vol. 27, pp. 1564-78.
22. F. R. N. Nabarro, Z. S. Basinski, and D. B. Holt: *Advances in Phys.*, 1964, vol. 13, pp. 193-323.
23. J. E. Dorn and S. Rajnak: *Trans. TMS-AIME*, 1964, vol. 230, pp. 1052-64.